Journal of Materials Chemistry B

# Multi-Functional Near-infrared Fluorescent Polymer Dot-siRNA for Gene Expression Regulation

| | |
|---|---|
| Journal: | *Journal of Materials Chemistry B* |
| Manuscript ID | TB-ART-08-2024-001954.R1 |
| Article Type: | Paper |
| Date Submitted by the Author: | 03-Dec-2024 |
| Complete List of Authors: | Sun, Di; University of North Dakota, Chemistry<br>Okosun, Blessing; University of North Dakota, Biology<br>Tayutivutikul, Kirati; University of North Dakota, Biology<br>Smith, Kaitlyn; University of North Dakota, Biology<br>Darland, Diane; University of North Dakota, Biology<br>Zhao, Julia; University of North Dakota, Chemistry |
| | |

# Multi-Functional Near-infrared Fluorescent Polymer Dot-siRNA for Gene Expression Regulation

*Di Sun[1], Blessing O. Okosun[2], Kirati Tayutivutikul[1,2], Kaitlyn H. Smith[2], Diane C. Darland[2*] and Julia X. Zhao[1*]*

[1.] Department of Chemistry, University of North Dakota, Grand Forks, ND, 58202

[2.] Department of Biology, University of North Dakota, Grand Forks, ND, 58202

*Co-Corresponding Authors

KEYWORDS: Nanomaterials, Polymer dots (Pdots), siRNA, Pdot-siRNA, Gene therapy, Gene silencing, Bioimaging, brain-derived microvascular endothelial cells and fibroblasts, pericytes.

ABSTRACT

Regulation of gene expression in eukaryotic cells is critical for cell survival, proliferation, and cell fate determination. Misregulation of gene expression can have substantial, negative consequences that result in disease or tissue dysfunction that can be targeted for therapeutic intervention. Several strategies to inhibit gene expression at the level of mRNA transcription and translation have been developed, such as anti-sense inhibition and CRISPR-Cas9 gene editing. However, these strategies have some limitations in terms of specificity, toxicity, and ease of use. We have designed a nanomaterials-based tool to inhibit gene expression in eukaryotic cells with a potential application in basic and biomedical research. At the heart of our rational design approach is a polymer dots (Pdots)-based nanoplatform that can provide a means to deliver gene-specific small interfering (siRNA) into cells while at the same time providing a visualization mechanism to determine which cells have taken up the siRNA. The Pdots that we designed and synthesized had an average size 64.25 ± 0.60 nm and a zeta potential that was +37.40 ± 8.28 mV. The Pdot-1 nmole Gapdh siRNA showed an average size of 82.27 ± 9.83 nm, with the zeta potential values determined to be -52.00 ± 6.05 mV in the HEPES buffer. Both Pdots and Pdot-siRNA displayed two emission peaks in the visible (588 nm) and near-infrared (NIR) emission range (775 nm). We treated primary cultures of mouse brain-derived microvascular cells with Pdot-Gapdh siRNA and observed uniform cellular uptake of the nanomaterial in the cells and reduced intensity of Gapdh immunolabeling. Our results highlight the potential application of Pdot-siRNA for gene expression targeting with simultaneous visual monitoring of Pdot-siRNA delivery. The simple design offers a flexible and novel strategy to inhibit a wide range of mRNA targets with minimal toxicity, high efficiency, and focused cell visualization.

## 1. INTRODUCTION

Historically, the three major treatment paradigms for cancer include surgery, chemotherapy, and radiotherapy. In the last decade, gene/immune therapy became the fourth avenue for cancer therapeutic strategies[1]. Compared to the three traditional treatment approaches, gene/immune therapy has shown fewer side effects and may provide higher cancer target efficiency[2, 3]. Other approaches have used anti-angiogenesis therapies in combination with chemo- and radiotherapy treatments, with mixed beneficial outcomes[4]. More recent efforts have focused on the development of gene silencing pathways for which RNA interference has emerged as a potential powerful tool for transcriptional/translational silencing of target genes[5-7]. Short interfering RNA (siRNA) is a short RNA of 20-25 base pairs (bp), which can directly disrupt targeted mRNAs and lead to downregulation of target gene expression[8]. Moreover, siRNA is negatively charged at physiological pH and can be combined with exterior cationic materials for biocompatible siRNA delivery for applications from basic research to clinical use[9, 10]. As a result, siRNA-mediated gene therapy may have promise as a therapeutic method.

One of the main challenges for siRNA gene therapy lies in the siRNA delivery process, itself. Factors contributing to inefficient delivery include poor stability of siRNA in circulation[11], siRNA degradation by nucleolytic enzymes[6], and siRNA destruction by self-immune recognition[6]. Therefore, improving the delivery efficiency of siRNA has become a critical factor for the development of siRNA-based gene therapy approaches. Suitable delivery platforms might provide protection for the siRNA, thus improving gene delivery efficiency. Traditionally, liposomes as well as inorganic and polymer materials have served as biomolecule-delivery platforms to control payload release, for example, in the context of drug encapsulation and release[12]. In this study, Li and colleagues constructed aromatized liposomes for systemic delivery, anticipated to extend the

duration of release and slow loss of particles from the site of injection[12]. Liposomes have a phospholipid bilayer structure to form spheres for drug loading to ensure a long circulation time; however, *in vivo* stability is a challenge for liposomes due to toxicity and poor local accumulation[13, 14]. Inorganic nanoparticles, such as carbon nanotubes, iron oxide nanoparticles, and mesoporous silica nanoparticles, have been utilized for drug delivery in a variety of systems[15, 16]. Although these inorganic nanoplatforms have shown good stability as delivery vehicles for anticancer drugs or siRNA, controllable drug or siRNA release and visual monitoring are often problematic.

To address these challenges, we developed a polymer-based matrix to form polymer dots (Pdots) as a delivery platform for siRNA (Pdot-siRNA). Due to the advantages of Pdots that include controlled release, protection, and specific targeting ability of biomolecules, Pdots may serve as an ideal nanocarrier for therapeutic agents such as conventional drug molecules or nucleic acid delivery[17, 18]. Our rationale was to leverage the advantages of siRNA-based inhibition of gene expression to engineer a nanomaterials-based platform to target specific genes. As a proof-of-concept, we have designed a Pdot-siRNA approach that offers specific inhibition of gene expression in combination with delivery visualization. We have tested this approach successfully in a primary culture of metabolically active brain microvascular-derived endothelial cells.

## 2. EXPERIMENTAL SECTION

### 2.1 Selection of polymers

The multi-functional tool was made using three polymers. The first is hydrophobic Poly[2-methoxy-5-(2-ethylhexyloxy)-1,4-phenylenevinylene] (MEHPPV), that is a semiconducting polymer with low molecular weight and hydrophobic characteristics. The second is Poly[2,6-(4,4-bis-(2-ethylhexyl)-4H-cyclopenta [2,1-b;3,4-b′]dithiophene)-alt-4,7(2,1,3-benzothiadiazole)] (PCPDTBD), that is a semi-conducting polymer. The third is a positively charged amphiphilic

polymer 1,2-distearoyl-sn-glycero-3-phosphoethanolamine-polyethylene glycol-polyetherimide (DSPE-PEG-PEI) that is synthesized using 1,2-distearoyl-sn-glycero-3-phosphoethanolamine-N-[succinimidyl (polyethylene glycol) -3400] (DSPE-PEG-NHS) and polyethylenimine (PEI, MW 25,000). The latter is a poly(phenylenevinylene) (PPV) derivative and a conjugating polymer with its highest occupied molecular orbital (HOMO) below the fermi level of gold. PCPDTBT is also a semiconducting polymer used to form a donor/acceptor (D-A) blend with a variety of conducting polymers which can be used to enhance the power conversion efficiency (PCE) in an electrochemical device[19]. Herein, we proposed to use it in a cell culture system to achieve biocompatible, fluorescence emission tool. MEHPPV can be blended with PCPDTBT for use as a sensitizer for dye sensitized photo sensors (DSPS).

2.2 Materials and instruments

The polymers MEHPPV, PCPDTBT, PEI, organic solvent tetrahydrofuran (THF), 4-(2-Hydroxyethyl)piperazine-1-ethanesulfonic acid, N-(2-Hydroxyethyl)piperazine-N′-(2-ethanesulfonic acid) (HEPES), dimethyl sulfoxide (DMSO), Amicon® Ultra-4 centrifuge filters with regenerated cellulose 100 K molecular weight cut-off (MWCO) and penicillin-streptomycin were purchased from Sigma Aldrich (St. Louis, MO, USA). DSPE-PEG-NHS, MW 3400 was purchased from NANOCS (New York, NY, USA). Deionized (DI) water (18 mΩ cm @ 25 ℃) was used in the experiments. Primary cultures of brain microvascular fibroblast cells (BMVFb) and brain microvascular endothelial cells (BMVEC) derived from CD1 adult mouse brain were purchased from Cell Biologics (Chicago, IL, USA). Dulbecco's modified Eagle medium with Glutamax (DMEM), Opti-MEM® Medium, Fetal Calf Serum, Penicillin-Streptomycin (10,000 IU Pen; 10,000 µg Strep in a 100X stock solution), Electron Microscopy Sciences (EMS) 16% Paraformaldehyde (PFA) aqueous solution, Phosphate buffered saline (PBS, 1X), cell culture

plates, 8-well chambered cover glass w/non-removable wells, 96-well plates, 4',6-diamidino-2-phenylindole (DAPI) (cat# 83210, 5 μg/mL), Alexa Fluor 488~phalloidin (cat# A12379, 1U in methanol), the Glyceraldehyde phosphate dehydrogenase (Gapdh) antibody (cat# MA1-16757, 1:100, 10 μg/mL), the donkey anti-rabbit IgG conjugated to Cy3 (cat# 711-166-152, 7.5 μg/mL), the Live/Dead Cell Imaging Kit, Invitrogen CyQUANTTM Lactate Dehydrogenase (LDH) Cytotoxicity Assay kit and Lipofectamine™ RNAiMAX Transfection Reagent were purchased from ThermoFisher Scientific (Waltham, MA, USA). The Maxwell® RSC simplyRNA extraction kit for cells was purchased from Promega (Madison, WI, USA). The immunolabeling block solution was prepared in the lab as previously described[20, 21]. The Vectashield hardset mounting medium was purchased from Vector Laboratories (Burlingame, CA, USA). Lab-Tek II 8-well Chamber Slides were purchased from Nalgene-Nunc International Corp (Naperville, IL, USA). Micro coverglass coverslips were purchased from Sargent-Welch VWR Scientific (Buffalo Grove, IL, USA). The cell counting system used was a LUNA-II Cell Counter from Logos (Biosystems, Annandale, VA).

A Hitachi 7500 transmission electron microscope (Hitachi, Tokyo, Japan) was used to observe the morphology of Pdots and Pdot-siRNA. At 25 ℃, the particle size and zeta potential of Pdots and Pdot-siRNA was determined using Zetasizer Nano-ZS dynamic light scattering (DLS) (Malvern Panalytical, UK) with a 633 nm Helium-Neon laser and backscattering detection. The fluorescence spectra and photostability measurements were obtained using a Shimadzu RF-6000 spectrophotometer (Shimadzu, Tokyo, Japan). UV-visible absorption studies were performed using a PerkinElmer Lambda 1050 UV-Vis-NIR spectrophotometer (Akron, OH, USA). An Olympus IX50/IX70 inverted system microscope (Olympus, Center Valley, PA) and captured using SimplePCI (v. 6.1) software. An Olympus FV3000 laser scanning confocal microscope

(Olympus, Center Valley, PA) was used for the *in vitro* cell immunolabel imaging of Pdots and Pdot-siRNA. Benchmark Multi-Therm™ shaker (Sigma Aldrich, St. Louis, USA) was used to conjugate DSPE-PEG-NHS with PEI. Branson sonicator 3800 (Emerson, St. Louis, USA) was used to help to synthesis of Pdots in the solution. The polymers' 1H-NMR spectra were detected using an AVANCE III spectrometer (HD 400 MHz, Bruker, Switzerland). A Thermo Fisher Scientific Nicolet iS5 Fourier transform infrared spectrometer (FT-IR) (Waltham, MA, USA) was utilized to obtain the IR spectra of DSPE-PEG-PEI, PEI, and DSPE-PEG-NHS. NuAire Biosafety level II sterile hood (model NU.425.400, NuAire, Plymouth, MN) was utilized for all cell culture experiments.

2.3 Synthesis of dual-emissive Pdots

Synthesis of positively charged DSPE-PEG-PEI amphiphilic polymer was based on the reaction between primary amine functional groups from PEI and the NHS ester moiety from DESP-PEG-NHS. Briefly, 0.8 mL of 10 mg/mL in DMSO was prepared in a 1.5 mL centrifuge tube, and then functionalized with 0.2 mL of 5 mg/mL DSPE-PEG-NHS in DMSO added into the above solution under shaking conditions for 24 h at 1000 rpm at room temperature. The resulting mixture was concentrated and purified using Amicon® Ultra-4 regenerated cellulose centrifugal filter with 100 K MWCO. The chemical structure of DSPE-PEG-PEI amphiphilic polymer was confirmed by $^{1}H$ NMR (in $D_2O$).

The dual-emissive Pdots were synthesized by using a nanoprecipitation method[22] with a minor modification. Briefly, 1.0 mg/mL of MEHPPV, 1.0 mg/mL of PCPDTBT were mixed in tetrahydrofluorane (THF) and 1.0 mg/mL of DSPE-PEG-PEI in DMSO were prepared as a working solution with 10.0 mL of DI water in a glass vial. Then, 1.0 mL of 1.0 mg/mL MEHPPV, 0.5 mL of 1.0 mg/mL PCPDTBT, and 0.1 mL of 1.0 mg/mL DSPE-PEG-PEI were mixed well

with rapid, repeated pipetting in 3.4 mL of THF, with the total volume set at 5.0 mL. The mixture was quickly injected into 10.0 mL of DI water under simultaneous ultrasonication (50 - 60 Hz) for 2 min. The THF solvent was evaporated off in the fume hood at room temperature overnight after which the Pdots solution in water was purified using a 0.22 μm VWR® syringe filter (VWR), following by centrifugation and concentration using Amicon® Ultra-4 regenerated cellulose centrifugal filter with a 100 K MWCO. The glass vial containing the final product in the 20 mM HEPES buffer was wrapped in tin foil to protect the nanomaterials from light, prior to storage at 4 ℃.

2.4 Electrostatic binding of siRNA with Pdots (Pdot-siRNA)

Based on their respective charges, the Pdots and siRNA are likely bound via an electrostatic interaction. The Pdots were synthesized using DSPE-PEG-PEI as an amphiphilic crosslinker and were positively charged in aqueous solution. Our current working model is that siRNA, which is negatively charged, will bind to positively charged Pdots to form the Pdot-siRNA complex. To generate the Pdot-siRNA, we used commercially available siRNA with two different sequences—Control siRNA and Gapdh-specific siRNA. Our rationale for this approach was to include a specific target siRNA (Gapdh) and a scrambled sequence Control siRNA for comparison. To generate the Pdot-siRNA, we combined 5.0 μg/mL Pdots and different amounts of siRNA (2 nmole, 1 nmole, 0.5 nmole, 0.25 nmole, 0.125 nmole and 0.0625 nmole) in HEPES buffer in centrifuge tubes under shaking conditions for 30 min at 4 ℃ at 200 rpm followed by incubation at 4 ℃ for 30 min. The final Pdot-siRNA was purified and centrifuged using the 100 K MWCO Amicon® Ultra-4 centrifuge filter. The characterization of the Pdots bound to the siRNA was investigated by UV-Vis absorption.

2.5 Cell Culture

Primary cultures of mouse-brain-derived microvascular fibroblast cells (BMVFb) and endothelial cells (BMVEC) were obtained from CD1 adult mouse brain and maintained in complete DMEM with 1X Glutamax and 4.50 g/L glucose supplemented with 10% fetal bovine serum (FBS), penicillin solution (100 U/mL), and streptomycin (100 µg/mL). The pellet was resuspended into 7.5 mL of complete DMEM with 15% FBS and 20 µg/mL Fibroblast growth factor 2 (Fgf2) along with penicillin-streptomycin 100 µg/mL stock solution. The cell lines were cultured at 37 ℃ under a humidified atmosphere containing 5% $CO_2$. Cell counts for assay plating were determined by counting a diluted suspension with a LUNA-II automated cell counter.

2.6 Efficacy test of siRNA

Commercially-available Control siRNA sequences (Cat. # 4390844 and 4390847, sequence proprietary) and Gapdh siRNA sequences (Cat. # 4390850, sequence proprietary) were obtained in lyophilized powder form and were resuspended with nuclease-free water to a stock concentration of 100 µM and stored at -20 ℃. To establish baseline efficacy for gene expression inhibition, BMVEC were seeded in a 24-well culture plate at ~50,000 cells per well and cultured for 48 h. The medium was removed and the cells were incubated in 0, 5, 10, and 20 µM Control or Gapdh siRNA with Lipofectamine® RNAiMAX Reagent as the delivery mechanism in Opti-MEM® Medium following the manufacturer's recommended protocol. After 4 h, the transfection mixture was removed and replaced with standard DMEM culture medium. After 24 h from the initial point of siRNA treatment, the medium was removed, the cells were washed once with 1X PBS on ice and the total RNA extracted using the Maxwell® RSC simplyRNA extraction kit for cells (Promega, Cat. # AS1390) following manufacturer's recommended protocol. In brief, cells were lysed in 200 µl of Thioglycerol and Homogenization Solution followed by treatment with DNase I Solution to eliminate contaminating genomic DNA. After RNA purification, the RNA

Integrity Number (RIN), as a reflection of RNA quality, and the concentration of the total RNA were determined using the High Sensitivity RNA ScreenTape system (Agilent Technology, 2200 TapeStation) and only samples with RIN ≥ 9.0 were used for generating complementary DNA (cDNA). In order to quantify changes in gene expression across samples, cDNA synthesis and quantitative PCR (qPCR) were conducted as described[21]. In brief, 200 ng of total RNA was mixed to a final concentration with 2.5 U/μL of Murine Moloney Leukemia Virus Reverse Transcriptase (MMLV-RT), 1.25 mM nucleotides, 0.5 mM oligo dT, 2.5 mM random Hexamers, 1 U/μL RNase Inhibitor, and 1X Reverse Transcriptase buffer and incubated for 1 h at 42 ℃ to generate the cDNA library. Library quality was confirmed based on uniform sample expression of the 18S Ribosomal subunit as a reference gene with primers as described in supporting materials (Table S2).

2.7 Pdots cellular uptake, signal persistence, and determination of *in vitro* cytotoxicity

To assess cellular uptake ability and determine toxicity, the effect of Pdots was evaluated at different concentrations in primary cultures of BMVFb cells. The BMVFb were cultured in 8-well Lab Tek Chamber slides at a target plating density of 2,500 cells/well. Four different incubation times (4 h, 8 h, 12 h, 24 h) were assessed with four different Pdots concentrations (20 μg/mL, 10 μg/mL, 5 μg/mL and control) in standard culture medium using four technical replicates for each time points and conditions. In brief, the cells were washed, fixed and blocked at each incubation time and concentration. The labelling mix included Alexa Fluor 488~phalloidin (1:300) and DAPI (1:1000) which was added to each slide. The slides were washed with 1X PBS and ProLong anti-fade mountant medium was added to each slide prior to coverslipping.

The cells were visualized using an Olympus FV3000 laser scanning confocal microscope under 20X objective and images were collected in each channel were postprocessed to generate composites using Adobe Photoshop. The DAPI signal (blue, detection wavelength 430-480 nm),

the Alexa Fluor 488 Phalloidin signal (green, 500-550 nm), and the Pdots (red, 550-650 nm) were collected from three independent images with 4 regions collected for each image. Cell viability under various incubation times and concentrations was summarized. Live and dead cells could be recognized based on the shape of nuclei. These images were analyzed with NIH Image J[23] to quantify the number of live cells (large, round nuclei) versus dead cells (small, pyknotic nuclei).

2.8 Determination of cellular uptake for Pdot-siRNA and immunolabeling

The BMVEC were cultured for 24 h in 8-well Lab Tek Chamber slides at a density of 50,000 cells/well to allow the cells to adhere fully to the plastic. The media was removed and replaced with 300 μL/well of freshly prepared Pdot-Control siRNA at different amounts of siRNA ranging from 0-2 nmole with an additional control well of 5 μg/mL of Pdots only. The cells were incubated with the Pdot-Control siRNA for 4 h to allow cellular uptake after which the media was removed, and the cells were fixed as described above. To visualize the cellular artchitecture, the cells were immunolabelled with block solution containing Alexa Fluor 488 phalloidin and DAPI. The control and treated cells were imaged using the Olympus FV3000 Laser Scanning Confocal Microscope (3 times line average, line sequential scan, Auto confocal aperture) and the objective lens was UPLFLN 40X oil with NA 1.3.

2.9 Investigation of *in vitro* Pdot-Gapdh siRNA effect in BMVEC

To determine if the Pdot-siRNA could be used to inhibit Gapdh expression, the BMVEC were cultured in a 24-well plate at a density of 50,000 cells/well and then treated with either Pdot-Control siRNA or Pdot-Gapdh siRNA for comparison. A comparison of Pdot alone (5 μg/mL), Control siRNA alone (1 nmole), Pdot-Control siRNA (0.5 and 1.0 nmole), and Pdot-Gapdh siRNA (0.5 and 1.0 nmole) was generated with four replicates for each condition. The cells were treated

in standard culture medium for 4 h, after which the treatment medium was removed and the cells were culture for an additional 20 h in normal growth media (DMEM with 10% FBS). After Pdot-siRNA treatment, cells were fixed in 4% PFA in PBS for 15 min at RT followed by additional PBS washes. Cells were blocked and permeabilized with 3% donkey serum, 1% bovine serum albumin (BSA), 0.1% saponin, 0.1% Triton X-100, and PBS for 30 min at RT. Cells were labelled with Gapdh antibody for 90 min at RT followed by three 10 min washes with PBS. Primary antibody was bound with donkey anti-rabbit IgG~Cy3 for 60 min at RT followed by three 10-min washes with PBS. Slides were mounted with ProLong anti-fade and a glass coverslip prior to confocal imaging as described above.

## 3. RESULTS AND DISCUSSION

### 3.1 Preparation of positively-charged DSPE-PEG-PEI amphiphilic polymer

The phosphoethanolamine-polyethylene glycol polymers (PE-PEG)-based nanoplatform is a promising nanoparticle delivery system because of its significant advantages, including biocompatibility, prolonged circulation, bioaccumulation in tumor cells and ability to readily incorporate drugs such as doxorubicin (DOX) to increase cancer cell internalization and enhance cytotoxicity[24-26]. DSPE-PEG-NHS provided an N-hydroxysuccinimide (NHS) ester for conjugation with amine-containing molecules/chemicals which was used to conjugate with PEI via the primary amine-reactive NHS ester moiety. The structure of DSPE-PEG-NHS, PEI, and the resulting DSPE-PEG-PEI copolymer were verified by $^{1}$H NMR (Figure 1). The deuterium oxide ($D_2O$) peak was detected at 4.8 ppm. The peaks of DSPE (1.0–1.5 ppm, stearoyl), PEG (3.7 ppm, -$CH_2O$-), NHS (2.7 ppm, -$NCOCH_2CH_2$-) and PEI (2.5–3.0 ppm, -$NHCH_2CH_2NH_2$) were confirmed using NMR spectroscopy. The$^{1}$H-NMR spectrum of DSPE-PEG-PEI in $D_2O$ exhibited characteristic peaks at 2.5–3.0 ppm were from methylene protons of PEI which was adjacent to

amine functional groups, indicating that PEI was successfully introduced to the DSPE-PEG-NHS molecule.

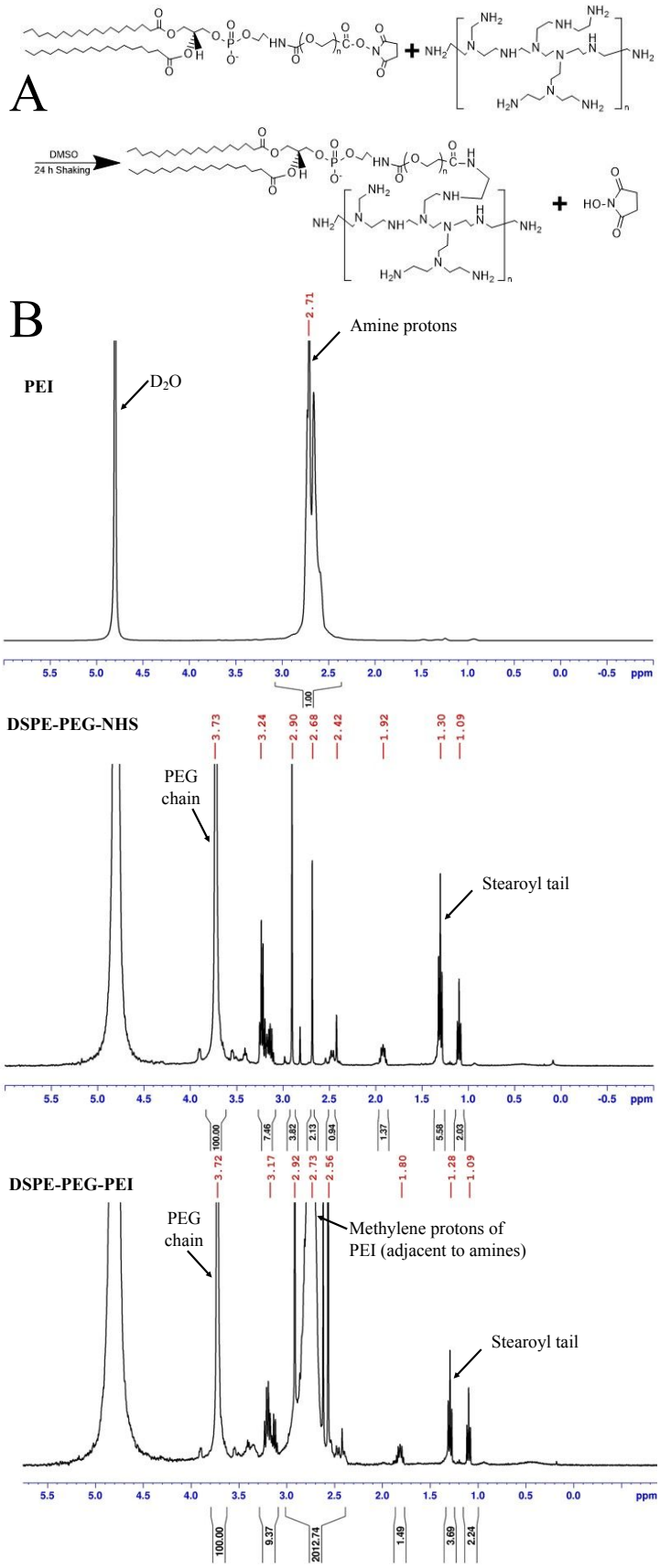
A
DMSO
24 h Shaking
B
PEI
D2O
Amine protons
2.71
DSPE-PEG-NHS
PEG chain
Stearoyl tail
3.73
3.24
2.90
2.68
2.42
1.92
1.30
1.09
DSPE-PEG-PEI
PEG chain
Methylene protons of PEI (adjacent to amines)
Stearoyl tail
3.72
3.17
2.92
2.73
2.56
1.80
1.28
1.09
ppm

Figure 1. Synthesis of DSPE-PEG-PEI amphiphilic polymer. (A) The synthetic route of DSPE-PEG-PEI polymer using starting materials including DSPE-PEG-NHS (MW 3,400) and PEI (MW 25,000) is shown. (B) $^{1}$H-NMR spectra of PEI, DSPE-PEG-NHS and DSPE-PEG-PEI is shown with the scale displayed in parts per million (ppm). Individual tracings are shown for each polymer component mix, and individual spectra are labeled with the ppm indicated for each. The 1H-NMR spectrum of DSPE-PEG-PEI in $D_2O$ exhibited characteristic peaks at 1.0-1.5 ppm (peaks of DSPE shown stearoyl tails), 2.5-3.0 ppm (peaks of PEI) and 3.7 ppm (peaks of PEG) indicating that PEI reacted with DSPE-PEG-NHS to form DSPE-PEG-PEI.

The FTIR spectra of DSPE-PEG-PEI, PEI, and DSPE-PEG-NHS was recorded in Figure 2. In the FTIR spectrum of DSPE-PEG-PEI and PEI, the peak at 3276 $cm^{-1}$, 1314 $cm^{-1}$, and 1016 $cm^{-1}$ were assigned to NH stretching vibration and bending vibration which represented the typical structure of the primary amine ($-NH_2$). The appearance of wide absorbance from 3400 to 3200 $cm^{-1}$ was attributed to the formation of an amide bond between carboxyl group and primary amine group after conjugation (Spectrum in black, top panel). The peak at 1712 cm $cm^{-1}$ from DSPE-PEG-NHS shifted to 1652 $cm^{-1}$ from DSPE-PEG-PEI indicated that the coupling reaction happened (Highlighted with the yellow bars). The peaks of three spectra at 2925-2810 $cm^{-1}$ were were attributed to the -CH, $-CH_2$ stretching vibration. The peak at 1456 $cm^{-1}$ in the PEI spectrum was ascribed to the stretching vibration of the C-N-H bond. The peaks between 1500-1400 $cm^{-1}$ visible on both DSPE-PEG-PEI and DSPE-PEG-NHS were assigned stretching vibration of carboxyl C=O. The bands at 1106 $cm^{-1}$ and 962 $cm^{-1}$ corresponded to symmetric and asymmetric C-O-C stretching which attributed to DSPE–PEG moiety (highlighted with the dash lines). The N-H out of plane wagging at 705 and 670 $cm^{-1}$ further confirmed the successful peptide conjugation (highlighted with the green bar). The FT-IR results analyzed here were consistant as have been

described in the literature[27-30]. The results indicated that amphiphilic polymer (DSPE-PEG-PEI) was successfully synthesized and PEI was successfully associated with DSPE-PEG-NHS contributing to the conjugated structure and functional groups of amphiphilic polymer.

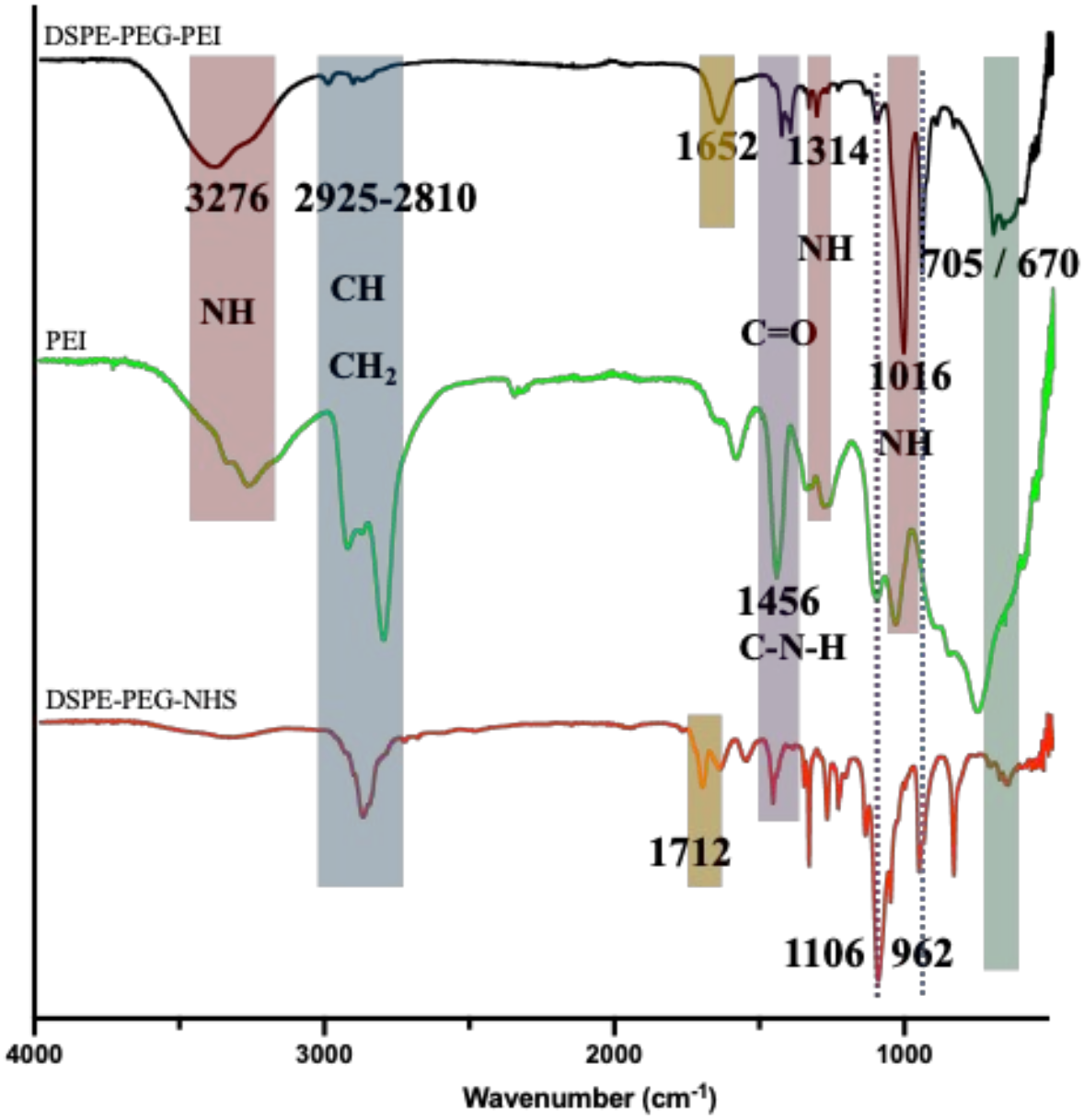


Figure 2. Chemical characterization of DSPE-PEG-PEI, PEI, and DSPE-PEG-NHS by using FT-IR. The results showed the functional peaks of the starting materials (DSPE–PEG-NHS, PEI) and

the product (DSPE-PEG-PEI). The black, green, and red curves showed the spectra of DSPE-PEG-PEI, PEI, and DSPE-PEG-NHS, respectively.

3.2 Rational design of Pdots for siRNA delivery

To develop a stable and multi-functional Pdots nanoplatform for siRNA delivery, we selected three types of polymers for the synthesis of Pdots, including hydrophobic Poly[2-methoxy-5-(2-ethylhexyloxy)-1,4-phenylenevinylene] (MEHPPV) and Poly[2,6-(4,4-bis-(2-ethylhexyl)-4H-cyclopenta [2,1-b;3,4-b′]dithiophene)-alt-4,7(2,1,3-benzothiadiazole)] (PCPDTBD), positively charged amphiphilic polymer 1,2-distearoyl-sn-glycero-3-phosphoethanolamine-polyethylene glycol-polyetherimide (DSPE-PEG-PEI). MEHPPV and PCPDTBT are semiconducting polymers with strong π-electrons, contributing to a donor-acceptor type conjugation system responsible for the absorption and emission of optical properties[31-33]. The rational design approach was to crosslink these two polymers together to increase the intensity of NIR fluorescence and generate a product that combined the advantages of both polymers in the final product. The DSPE-PEG-PEI was synthesized using 1,2-distearoyl-sn-glycero-3-phosphoethanolamine-N-[succinimidyl (polyethylene glycol)-3400] (DSPE-PEG-NHS) and polyethylenimine (PEI, MW 25,000), and NHS ester can be easily incorporated into liposome and other chemicals via the reaction of NHS and amine groups. DSPE-PEG-PEI can both provide a positively-charged surface on the Pdots and act as backbones in the Pdots to support stable and crosslinked nanoparticle formation.

The synthesis approach to generate Pdots is based on the nanoprecipitation method as shown in the schematic (Figure 3A). In brief, 1.0 mL of 1.0 mg/mL MEHPPV and 0.5 mL of 1.0 mg/mL PCPDTBT were mixed in a water-miscible organic, solvent-tetrahydrofuran (THF). 0.1 mL of 1.0mg/mL amphiphilic polymer DSPE-PEG-PEI in DMSO was added to the polymer mixture above. A total of 5.0 mL of these polymer solutions were mixed well and rapidly added to an

excess of 10.0 mL DI water under 50-60 Hz ultrasonic dispersion conditions for 2 min. Due to the presence of the amphiphilic polymer DSPE-PEG-PEI, Pdots have amine functional groups on the surface and can be dispersed in the aqueous solution. The current model of how the Pdot-siRNA is taken up and works in cells is as follows. The 3' phosphate group on the ribonucleotide strand confers a negative charge; therefore, the siRNA electrostatically binds to the outside surface of the Pdot nanoplatform that is positively-charged (Figure 3B). When the Pdot-siRNA complex is taken up by the cells, the complex may be encapsulated within an endosome structure and delivered to the perinuclear region of the cell via a putative mechanism that has been described previously in the literature[34]. Once the Pdot-siRNA has escaped the endosome compartment, the siRNA will be released from the Pdots nanoplatform and bind to its mRNA target via base-pair complementarity. Binding of the siRNA to its specific target will prevent translation by the ribosomal complex or target the double-stranded RNA for degradation, resulting in reduced protein product for that target transcript. This approach allows for the dual advantage of being able to deliver siRNA specific to critical cellular targets and modify gene expression while simultaneously imaging exactly where the siRNA has been delivered. Depending upon the potential application, this tool may have broad use in basic and clinical research.

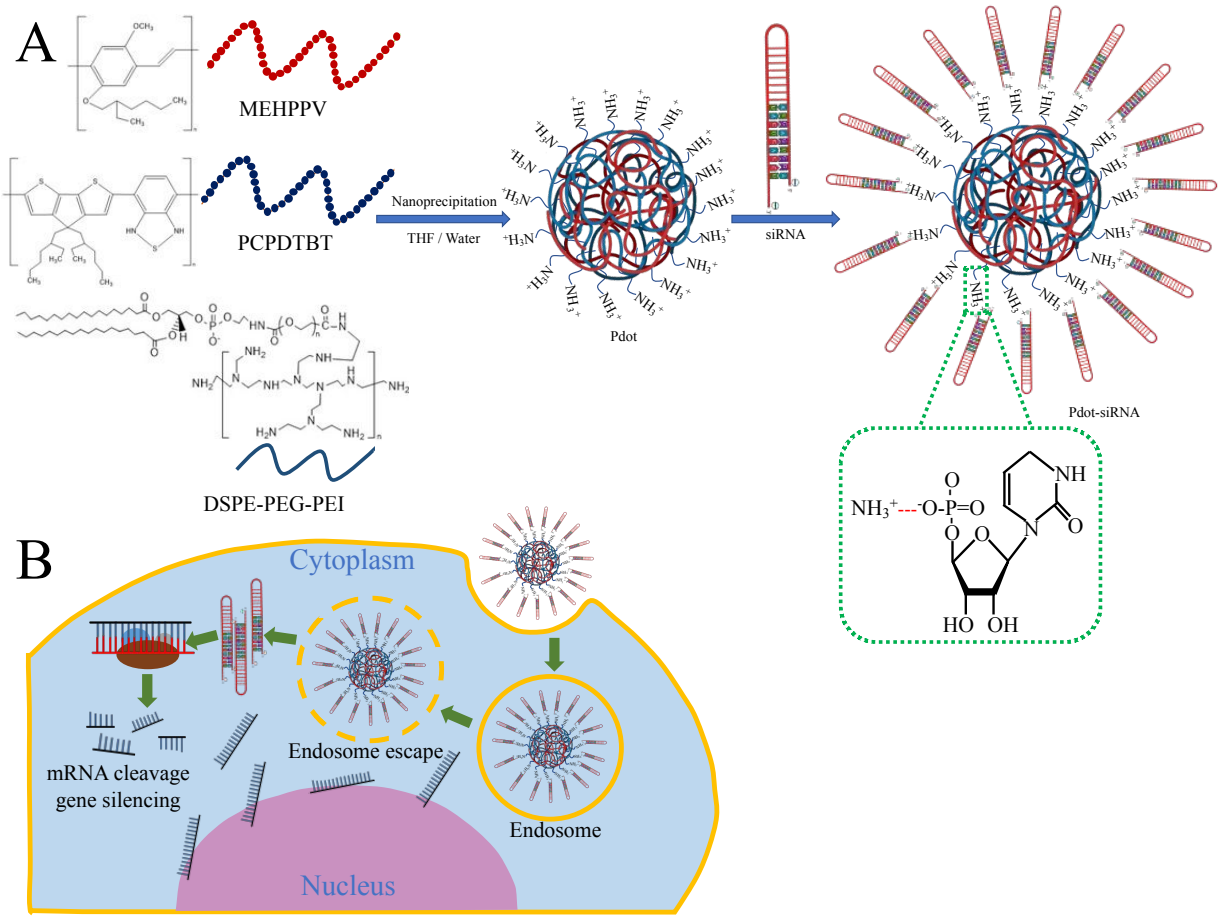


Figure 3. Formation of Pdots and Pdot-siRNA and the potential delivery mechanism to the cell. (A) The schematic diagram shows the synthesis of Pdots and binding with siRNA around the Pdots. The dashed box depicts a potential model for how the Pdots and siRNA may be connected through electrostatic interactions. (B) Schematic illustration of our current working model regarding how the Pdot-siRNA nanoplatform may undergo cellular uptake and siRNA delivery to target transcripts.

3.3 Characterization of Pdots and Pdot-siRNA

The morphology and surface charge of Pdots, Pdot-Control siRNA, and Pdot-Gapdh siRNA were characterized using TEM and DLS (Figure 4) based on the nanomaterials dispersed in HEPES buffer. The TEM images showed that Pdots, Pdot-Control siRNA, and Pdot-Gapdh

siRNA were successfully synthesized and dispersed in the solution without aggregation. The hydrodynamic diameter of Pdots was measured to be 64.25 ± 0.60 nm with positively-charged zeta potential (+37.40 ± 8.28 mV) around the surface in HEPES buffer (Figure 4A). The diameter of Pdots with 0.5 nmole of Control siRNA and Pdots with 1.0 nmole of Control siRNA were measured to be 75.05 ± 3.46 nm and 77.66 ± 1.05 nm, with the zeta potential of each being negatively-charged at -37.00 ± 10.07 mV and -18.37 ± 0.25 mV, respectively (Figure 4B, 4C). In comparison, the diameter of Pdots with 0.5 nmole of Gapdh siRNA and Pdots with 1.0 nmole of Gapdh siRNA was measured to be 84.50 ± 8.45 nm and 82.27 ± 9.83 nm, with the zeta potential values determined to be -45.77 ± 7.16 and -52.00 ± 6.05 mV, respectively (Figure 4D, 4E). The average size comparison between Pdots and different amounts of Pdots bound to Control or Gapdh siRNA was shown in Figure 4F. As expected, Pdots were positively-charged; however, when Pdots bound with Control or Gapdh siRNA the overall zeta potential was negative (Figure 4G). The polydispersity index (PDI) confirmed that Pdots had a narrow particle size distribution in HEPES buffer, and Pdots with siRNA showed a relatively high particle size distribution (Figure 4H). During the characterization of thePdots and Pdot-siRNA, absorbance, size, and zeta potential were measured in water, biocompatible buffer (HEPES and PBS), and cell culture medium (DMEM). This latter series of control tests revealed that the nanomaterial average diameter differed in buffer versus cell culture media (Figure S1 & Table S1).

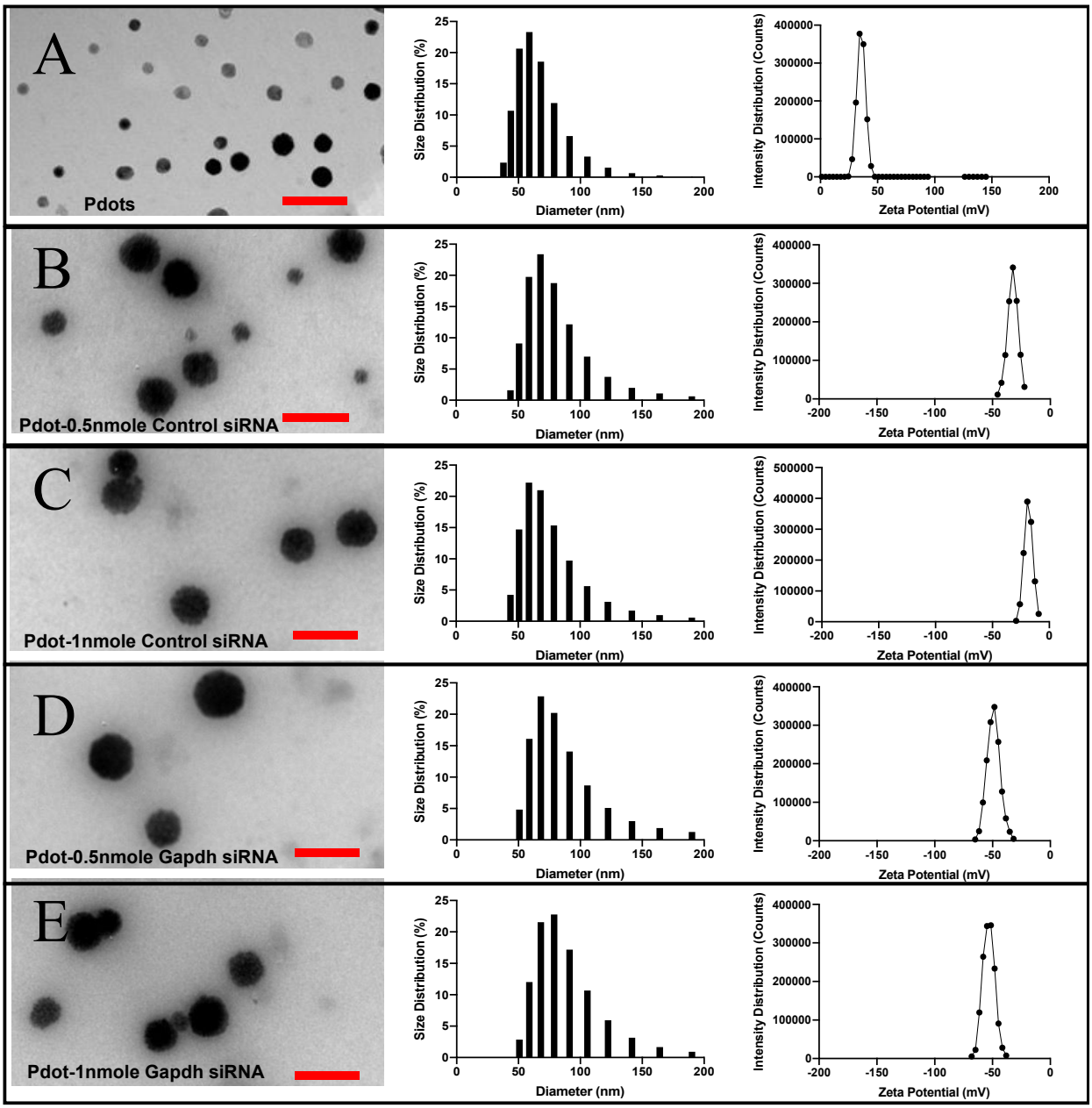
A
Pdots
B
Pdot-0.5nmole Control siRNA
C
Pdot-1nmole Control siRNA
D
Pdot-0.5nmole Gapdh siRNA
E
Pdot-1nmole Gapdh siRNA
Size Distribution (%)
Diameter (nm)
Intensity Distribution (Counts)
Zeta Potential (mV)

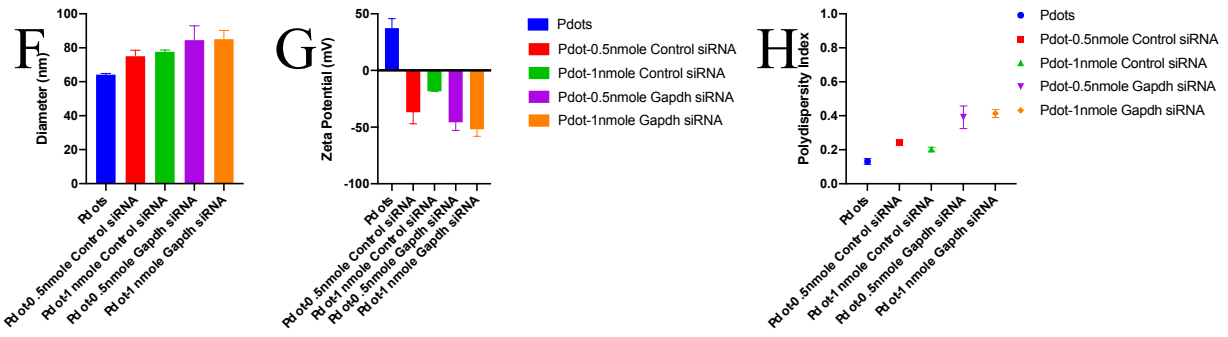
F
Diameter (nm)
G
Zeta Potential (mV)
H
Polydispersity Index
Pdots
Pdot-0.5nmole Control siRNA
Pdot-1nmole Control siRNA
Pdot-0.5nmole Gapdh siRNA
Pdot-1nmole Gapdh siRNA

Figure 4. Morphology investigation of Pdots and Pdot-siRNA in HEPES buffer. (A) TEM image, size distribution, and zeta potential of Pdots. (B) TEM image, size distribution, and zeta potential of Pdot-0.5 nmole Control siRNA. (C) TEM image, size distribution, and zeta potential of Pdot-1.0 nmole Control siRNA. (D) TEM image, size distribution, and zeta potential of Pdot-0.5 nmole Control siRNA. (E) TEM image, size distribution, and zeta potential of Pdot-1.0 nmole Gapdh siRNA. (F) Average size comparison of Pdots and Pdot-siRNA. (G) Average zeta potential comparison of Pdots and Pdot-siRNA. (H) Average PDI comparison of Pdots and Pdot-siRNA. The red scale bar is 0.2 μm in A-E.

In addition to the delivery function of the Pdots nanoplatform, there is also a potential advantage from the real-time monitoring and detection via fluorescence emission of the Pdots. In order to determine the Pdots' absorbance and emission properties, we first investigated a concentration series from 1 μg/mL to 10 μg/mL using a UV/Vis/NIR spectrometer (Figure 5A). The absorbance spectra showed two absorbance peaks at 500 nm and 693 nm, respectively. Linear regression analysis predicted the Pdots' concentration based on absorbance value. A linear relationship for both 500 nm and 693 nm, relative to concentration, with R square equal to 0.9961 and 0.9832 (Figure 5B and 5C), respectively, indicates a tight correlation between these two parameters. Once the siRNA was associated with the Pdots, an additional peak at 257 nm was observed, which is characteristic of nucleotide absorbance properties. The spectra of solo Control siRNA and Gapdh siRNA showed in Figures 5D and 5E further confirming that Pdots were successfully bound with siRNA. These results indicate that siRNA bound to Pdots shifts the absorbance properties to include that associated with the nucleotides for both Control siRNA (Figure 5D) and Gapdh siRNA (Figure 5E).

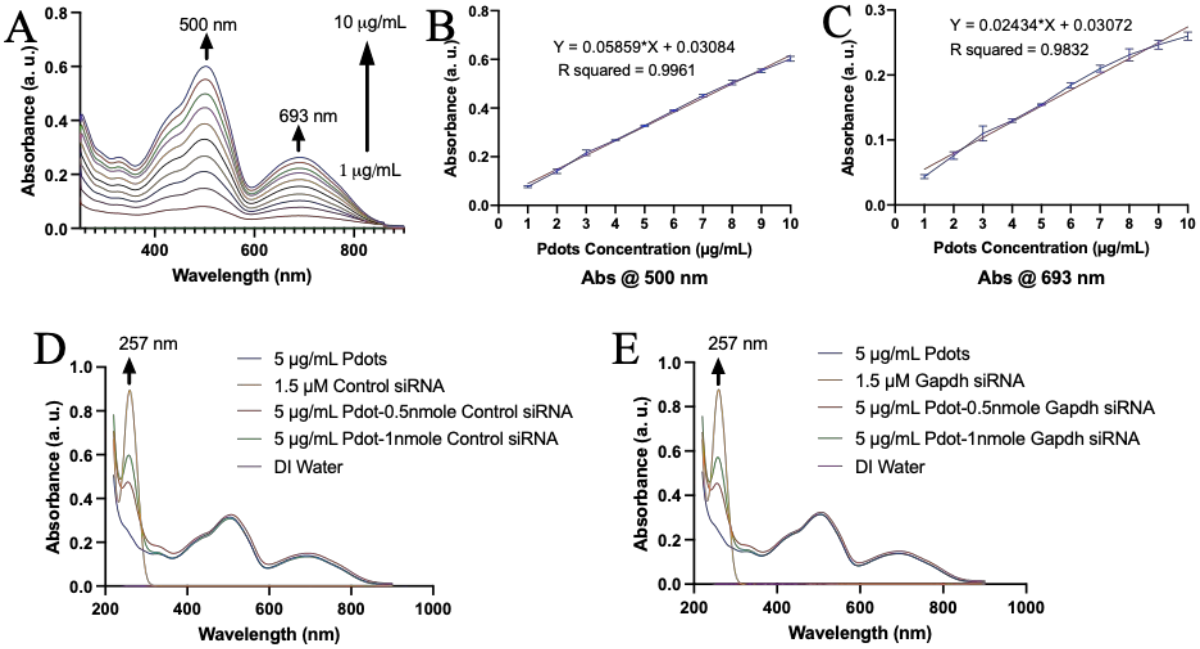


Figure 5. Absorbance properties of Pdots, Pdot-Control siRNA, and Pdot-Gapdh siRNA. (A) Absorbance properties of Pdots under a concentration series from 1 μg/mL to 10 μg/mL. (B) Linear regression analysis of different concentrations of Pdots versus absorbance peak at 500 nm. (C) Linear regression analysis of different concentrations of Pdots versus absorbance peak at 693 nm. (D) Absorbance property of Pdots with a certain amount (0.5 nmole and 1.0 nmole) of Control siRNA. (E) Absorbance property of Pdots with a certain amount (0.5 nmole and 1.0 nmole) of Gapdh siRNA.

Fluorescence excitation and emission of Pdots under different concentrations are shown in Figure 6. The spectra showed that Pdots had two emission peaks at 588 nm and 775 nm, with the excitation set at 500 nm (Figure 6A). The two emission peaks were generated from MEHPPV and PCPDTBT, respectively. The absorbance result showed two absorbance peaks at 500 nm and 693 nm, respectively. The fluorescence properties of the Pdots were also investigated using 693 nm as the fixed excitation wavelength and run as an emission spectra series. When the emission was set at 775 nm, and the excitation spectra series run, the excitation peak fluorescence

intensity at 500 nm had a similar intensity compared with the emission peak fluorescence intensity at 775 nm (Figure S2). Overall, there were two excitation peaks at 500 nm and 693 nm, respectively, and two emission peaks at 588 nm and 775 nm, respectively. The two emission peaks had a good linear relationship under a concentration series of Pdots with R square equal to 0.9747 under emission peak at 588 nm and 0.9917 under emission peak at 775 nm (Figure 6B, 6C). It is likely that the energy transfer between MEHPPV and PCPDTBT resulted in the excitation and emission peak and intensity shift observed. This type of shift has been detected with similar polymers in previous research[35].

In order to determine how the binding of the siRNA affected the fluorescence properties of the Pdots, we quantified fluorescence intensity across different amounts of Pdots bound to either Control siRNA or Gapdh siRNA. The Pdots bound to siRNA had similar fluorescent intensity compared to Pdots alone (Figure 6D). Both Pdot-Control siRNA and Pdot-Gapdh siRNA had two excitation peaks at 500 nm and 693 nm and two emission peaks at 588 nm and 775 nm (Figure S3).

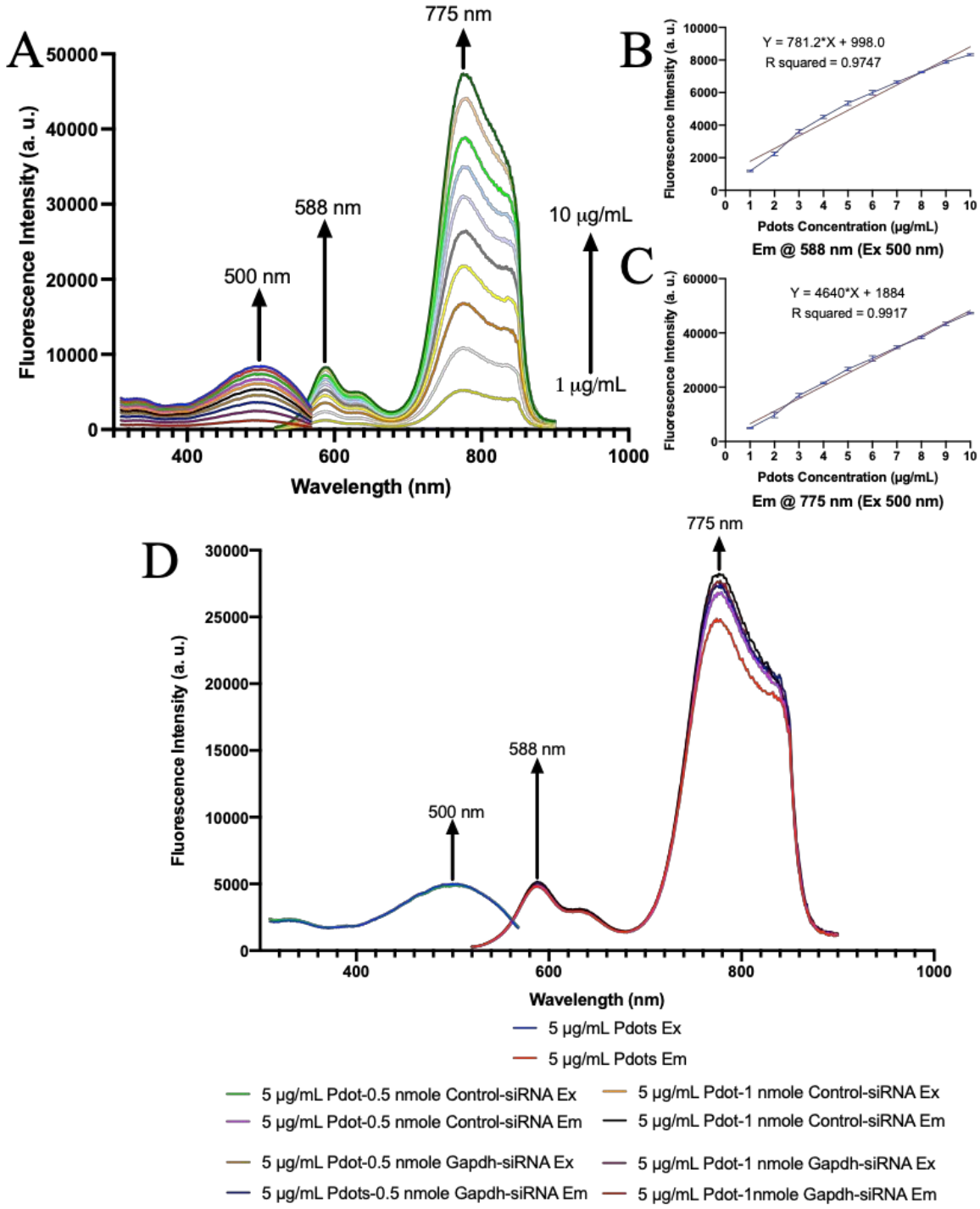


Figure 6. Fluorescence properties of Pdots in a dose series from 1 μg/mL to 10 μg/mL. (A) Fluorescent spectra of Pdots through fix excitation at 500 nm and emission at 588 nm. (B) Linear regression analysis of a series concentrations of Pdots versus emission fluorescence intensity at

588 nm while excitation was fixed at 500 nm. (C) Linear regression analysis of a concentration series of Pdots versus emission fluorescence intensity at 775 nm with excitation fixed at 500 nm.

3.4 Assessment of Pdots *in vitro* labeling and cytotoxicity

To optimize cellular uptake ability and evaluate the cytotoxicity of Pdots, we tested a rapidly dividing primary culture cell type, brain micro-vascular fibroblast (BMVFb) cells. Typically, vascular fibroblast cells are recruited to the perivascular space near endothelial cells, differentiate as pericytes and contribute to vascular stability, making them ideal for testing cytotoxicity[36]. Moreover, fibroblasts are easy to grow in culture and they also have the ability to produce factors that facilitate endothelial cell (EC) growth and maturation[37]. BMVFb were plated at a density of 2,500 cells/well in 8-well chamber slides in a time course series of treatment times (4, 8, 12, and 24 h) and differing Pdots concentrations (20, 10, 5, and 0 μg/mL) to determine optimal uptake and minimal labeling dose requirements. After the different Pdots treatment time periods, the medium was switched back to normal growth medium and the cells were fixed, washed, labeled and imaged as described above.

The Pdots were readily taken up by the BMVFb (red) and easily visualized in comparison with the actin cytoskeleton (green) and the nuclei (blue) after a 4 h exposure time (Figure 7) with the brightness of the Pdots fluorescence increased at the higher concentrations of Pdots (compare 5 to 20 μg/mL). The BMVFb cells incubated without Pdots had no signal in the red channel (control panels). The red arrows highlight select cells with clear, round nuclei with the Pdots fluorescent signal localized to the perinuclear region of the cytoplasm (yellow circles). Treatment of the BMVFb cells with 20 μg/mL Pdots resulted in numerous cells with small, round or condensed and pyknotic nuclei (white arrows). The BMVFb cells incubated with Pdots for 8 h under different concentrations showed a similar phenomenon (Figure S4); however, the

small, round and pyknotic nuclei were more abundant in the cultures treated with 10 μg/mL Pdots suggesting increased cellular sensitivity with a longer exposure to Pdots.

Similar results were observed after an 12 h treatment window, with the numbers of dead (pyknotic nuclei) and dying (small, round nuclei) cells increasing. In contrast, cells appeared healthy after treatment with 5 μg/mL Pdots(Figure S5). When BMVFb cells were incubated with different concentration of Pdots for 24 h the intermediate and pyknotic nuclei were substantially increased at the 5 μg/mL dose. The dead cells increased at 10 μg/mL with almost 100% toxicity at the 20 μg/mL dose (Figure 8). We suspect that the toxicity comes from the alteration associated with the osmolarity of the cell culture medium. When the Pdots are generated, the initial preparation is done in water and then the Pdots are concentrated so that we can dilute to a range tolerable to cells in culture medium. During the coculture of the cells and nanoparticles, the increase in the concentration of exogenous Pdots also increases the buffer solution, which affects the culture medium and causes a sharp change in the osmolarity of the cell environment.

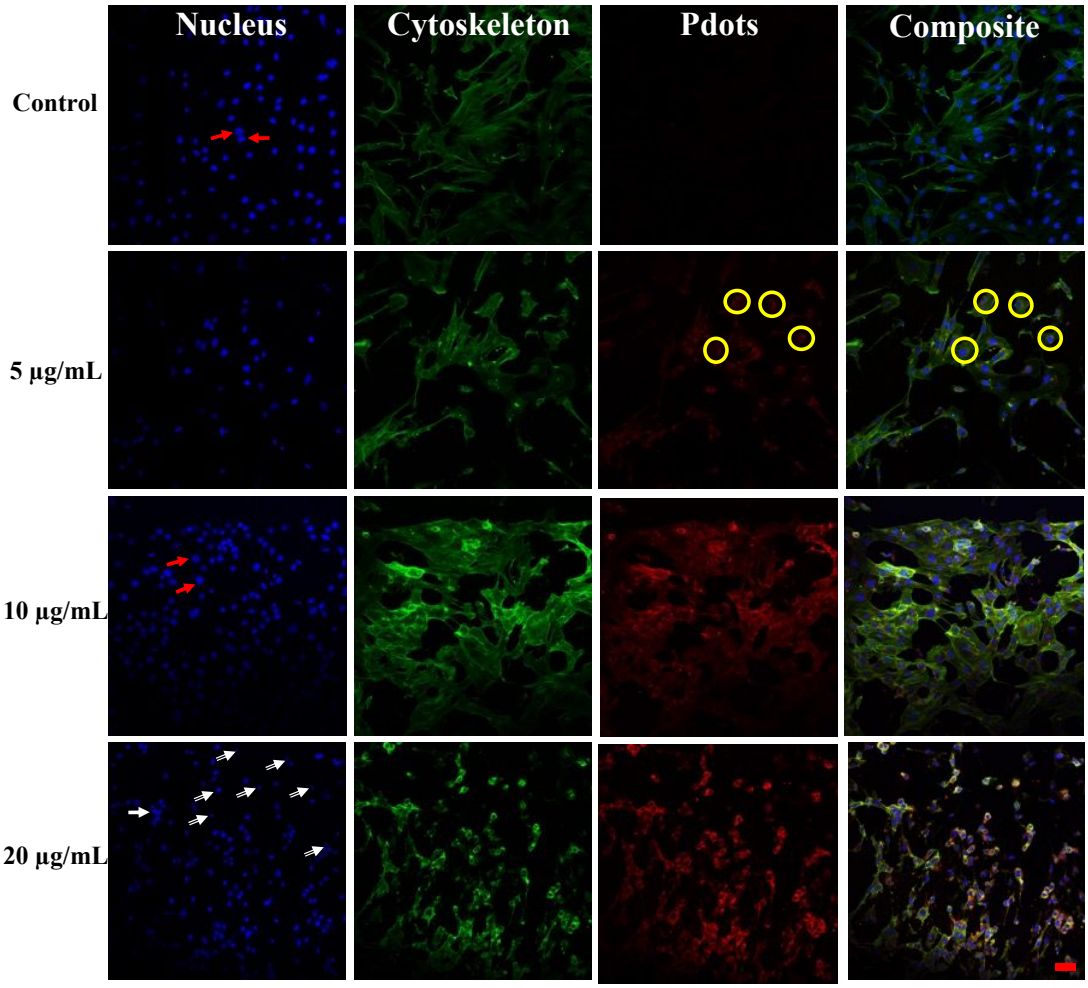


Figure 7. Imaging of BMVFb cells incubated with Pdots for 4 h. BMVFb were cultured in 8-well Lab Tek Chamber slides at a target plating density of 2,500 cells/well, treated with different concentrations of Pdots (red) for 4 h and then post-fixation labeled with DAPI (blue, nuclei) and Alexa Fluor 488 phalloidin (green, actin). The red arrows indicated healthy cells with normal-sized, round nuclei while the white arrows indicate an intermediate stage of cell that is likely undergoing cell death (small, round nuclei) or is already pyknotic. The yellow circles indicated the perinuclear Pdots fluorescent signal. The scale bar is 50 μm for all panels and the three-channel overlay is shown for comparison with the individual channels.

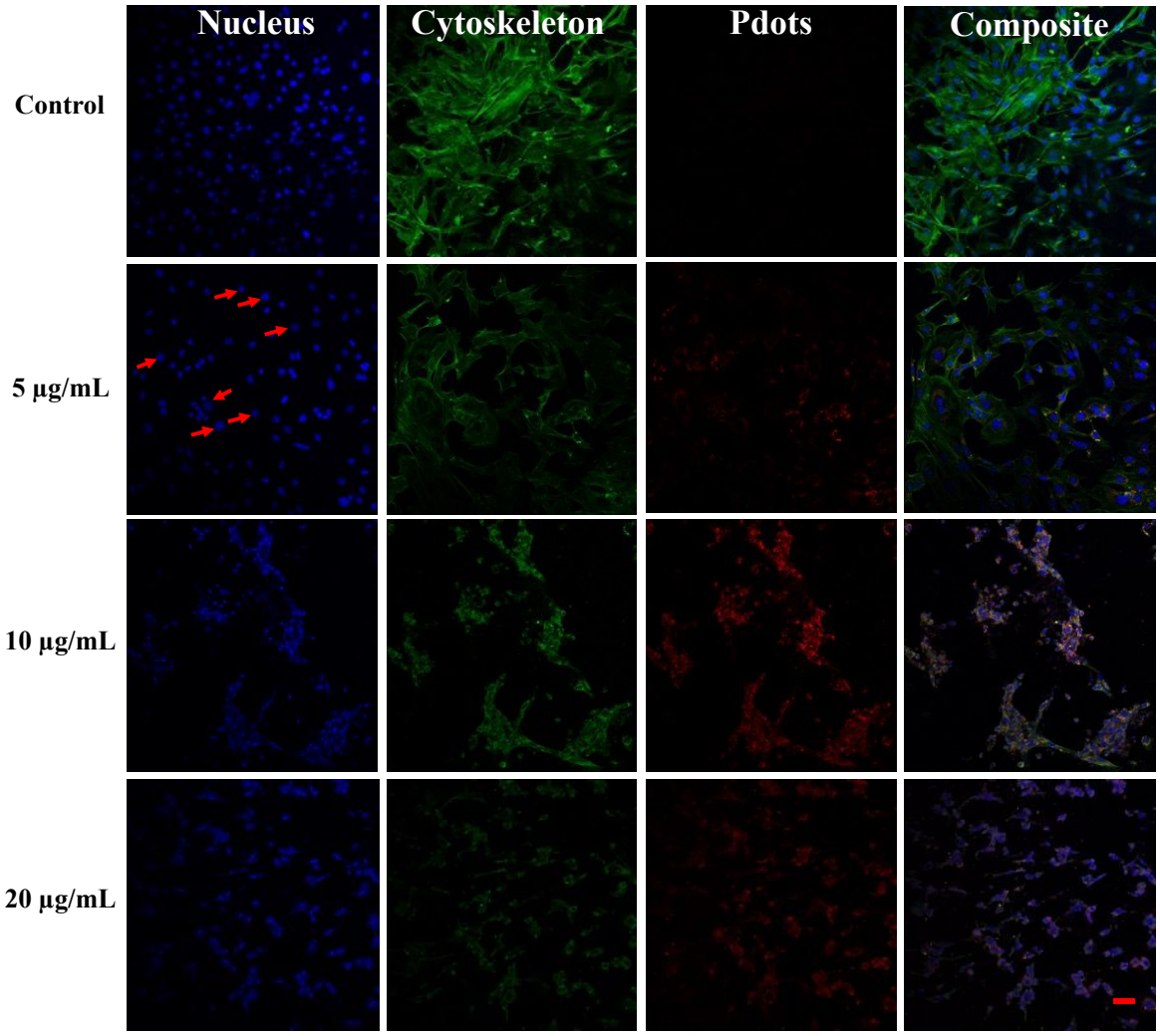


Figure 8. Imaging of BMVFb cells incubated with Pdots for 24 h. BMVFb were cultured as described for Figure 6 but were incubated with varying Pdots concentrations for 24 h and then post-fixation labeled with DAPI (blue, nuclei) and Alexa Fluor 488 phalloidin (green, actin). The red arrows indicated that there were still healthy cells with normal-sized and round nuclei after treatment with 5 μg/mL of Pdots. The scale bar is 50 μm in all panels.

3.5 Cell viability under different incubation times and concentrations of Pdots

Live and dead cells were recognized based on the shape of nuclei uder various incubation times and concentrations. As shown in Figure 9A, Pdots had no significant toxicity lower than 10 μg/mL, and the percentage of cell viability was 83.3% under the highest concentration at 20

μg/mL. Pdots showed less toxicity under high concentration at 20 μg/mL with short incubation time at four h. With increasing incubation time, cell toxicity increased, and cell viability was 56.3% and 85.8% at 20 μg/mL and 10 μg/mL, respectively, for the 8 h incubation period (Figure 9B). Cell toxicity was increased at 20 μg/mL with 12 h incubation with cell viability dropping to 4.1%, in contrast to the cell viability at 81.3% with 10 μg/mL treatment (Figure 9C). After the cells were incubated with Pdots for 24 h, the majority of the cells were dead with 20 μg/mL treatment (Figure 9D).

Overall, 4 h incubation of BMVFb with Pdots was an ideal time for cell uptake with the least amount of toxicity. The fluorescent signal from the Pdots was distributed around the nuclei in the cytoplasm but was not detected inside the nuclei. At a dose of 20 μg/mL, the Pdots were always toxic, and 10 μg/mL of Pdots showed toxicity at 8 h treatment and beyond. 5 μg/mL of Pdots were minimally toxic, but the fluorescent signal was not as bright as that of the Pdots at 10 μg/mL. The 10 μg/mL of Pdots at 4 h showed the optimal combination of minimal toxicity with strong fluorescence intensity.

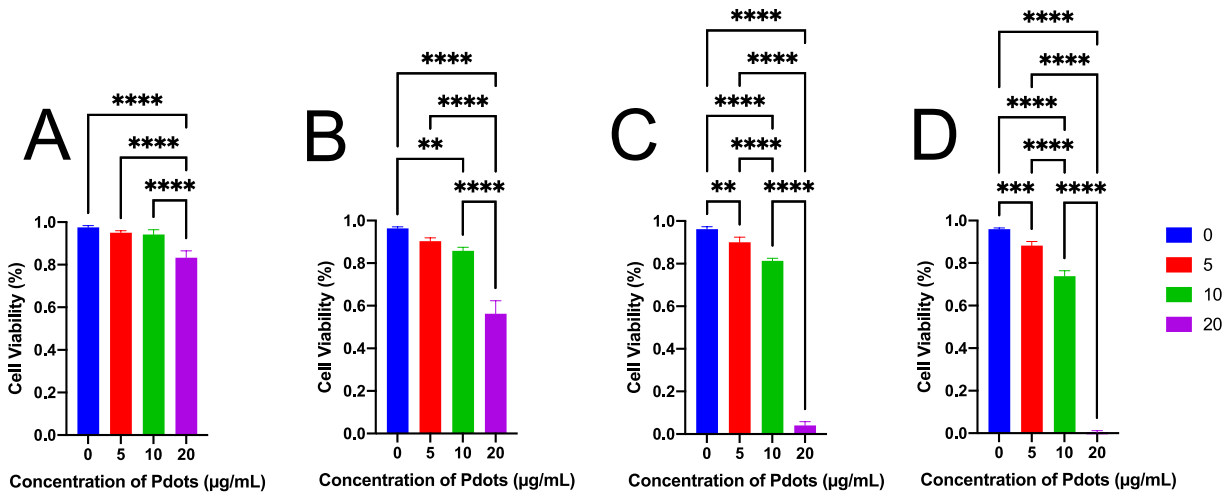


Figure 9. Summary of cytotoxicity under different incubation times with different concentrations of Pdots on BMVFb cells. Pdots were incubated with the cells for 4 h (A), 8 h (B), 12 h (C), or

24 h (D) at the concentrations indicated on the x-axes. Data are presented as the mean ± SD, n=3. The one-way ANOVA showed significant differences comparing the highest concentration of Pdots (20 μg/mL) with the lower concentration of Pdots and control, although cell viability for all concentrations closely matched controls. The pair-wise analysis with Tukey multiple comparisons *post hoc* test showed significance with bars indicating a comparison: $p < 0.01$ was presented as **, $p < 0.001$ was presented as ***, and $p < 0.0001$ was presented as ****.

3.6 Determining the duration of Pdots fluorescent signal in cultured cells

Since the incubation time and different concentrations of Pdots with BMVFb had been optimized, we wanted to determine how long the Pdots fluorescent signal were persist over time in culture. After a 4 h incubation with 10 μg/mL of Pdots, the BMVFb were transitioned back to normal growth medium and and maintained for 14 days. The day of plating was considered day 0 for the time series with time points collected every two days thereafter. The cells were labeled with DAPI to bind to the minor groove of DNA in the nuclei and Alexa Fluor 488 phalloidin to bind to the actin cytoskeleton to visualize the relative location of Pdots in the cells. Confocal images were captured from different time points (Figure S6). From 0-day until 8-days, the fluorescent signal from the Pdots (red channel) was readily detected in the cells. Interestingly, as the cells underwent normal division, the fluorescent Pdots signal was dispersed to the daughter cells and remained visible throughout the culture. A weak fluorescent signal was detected up until 10 days in culture. This result suggests that Pdots can be applied as a tool for siRNA delivery and can also be tracked regarding their long-term fluorescent signal in cultured cells.

3.7 Determining cellular uptake for Pdot-siRNA in BMVEC

While BMVFb cell images provided a unique opportunity to test the biocompatibility of the cell with Pdots in a rapidly dividing population, BMVEC provided another vascular cell

population in which to test this novel tool. The vascular endothelium is critical in regulating the interaction of circulating cells with the blood vessel wall. Vascular EC imaging can provide information about the vasculature's permeability and or the vessels' functional abnormalities. To expand the type of cell that we tested for bioimaging and investigate the amount of Pdot-siRNA that can be taken up by the cells we tested our Pdot-siRNA in BMVEC. Optimal time course and siRNA concentration were determined in BMVEC (Figure S7). Pdots loaded with different Control siRNA amounts were incubated with BMVEC for 4h. The cells were fixed and immunolabeled with DAPI and then imaged using an Olympus BX51WI fluorescence microscope. As shown in Figure 10, the BMVEC incubated without Pdots showed no fluorescence in the cytoplasm, as expected. BMVEC incubated with Pdots displayed the expected emission (green fluorescence, detection range 550-650 nm) as well as NIR (red channel, detection range 700-800 nm) imaging pattern since Pdots have two emission peaks at 588 nm and 775 nm. Pdots with different amounts of Control siRNA, including 2nmole, 1 nmole, 0.5 nmole, 0.25 nmole, 0.125 nmole, and 0.0625 nmole, displayed a similar cytoplasmic labeling pattern when compared to cells treated with Pdots alone as was observed with BMVFb. Immunolabeling results verified that the Pdot-siRNA provided a robust signal, localized primarily around the nucleus and throughout the cytoplasm for BMVEC.

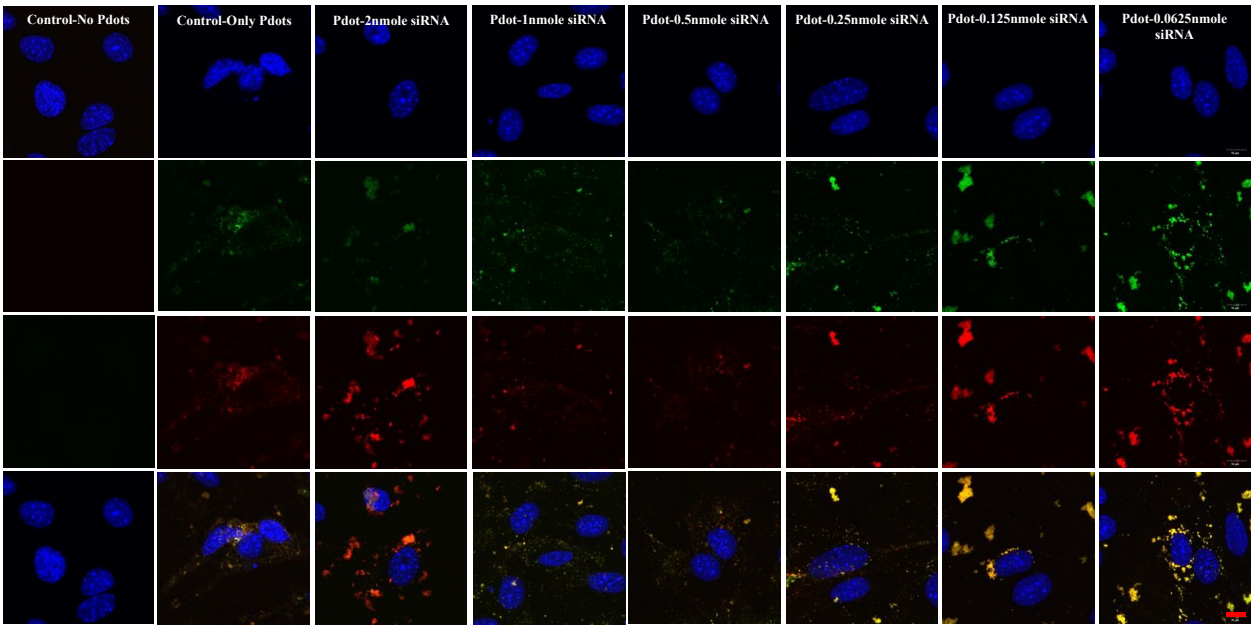


Figure 10. BMVEC incubated with Pdots and Pdots with different amounts of Control siRNA for 4 h. The cells were fixed and labeled with DAPI (blue nuclei). The green channel was a fluorescent signal from Pdots, with a set detection range from 550-650 nm. The red channel was a fluorescent signal from Pdots, with a set detection range from 700-800 nm. The scale bar was 10 μm.

3.8 Investigation of Gapdh target gene expression

In order to determine if the Pdot-Gapdh siRNA is able to inhibit the expression of the target gene, Gapdh, we assessed changes in Gapdh protein via immunolabeling (Figure 11). BMVEC were plated in 24-well cell culture plates at a density of 50,000 cells/well and allowed to adhere for 24 h. Cells were then treated with Pdots without siRNA, Pdot-Control siRNA, and Pdot-Gapdh siRNA at two different concentrations for 4 h. Cells were transitioned to complete DMEM for an additional 20 h prior to being collected for Gapdh immunolabeling (Figure 11). The Gapdh was detected throughout the cytoplasm of the cells and pronounced in the perinuclear region (green channel) in both control conditions (Pdots, Pdot-Control siRNA; left panels). The labeling intensity was reduced in cultures treated with Pdot-Gapdh siRNA (Figure 11, right

panels). Pdot detection in two distinct emission spectra, 550-650 nm (red violet channel) and NIR 700-800 nm (red channel), were consistent with previous results to localize the Pdots in the cells.

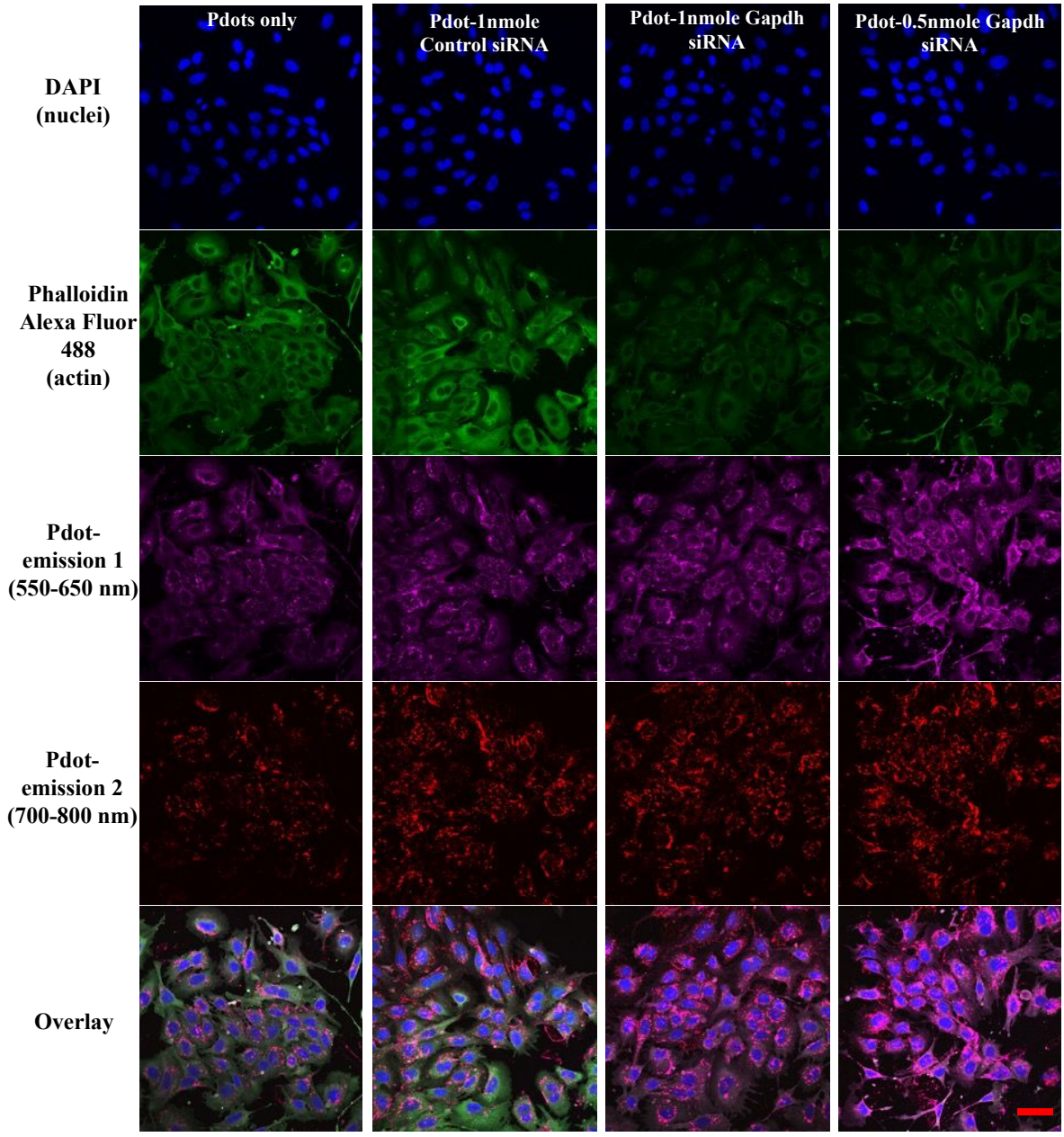


Figure 11. Gapdh immunolabeling has lower intensity in BMVEC treated with Pdot-Gapdh siRNA compared to Pdots and Pdot-Control siRNA. The BMVEC were labeled with Gapdh antibody (green channel) and with DAPI (blue nuclei) across all treatment conditions. The

fluorescent signal from Pdots was detected in two emission ranges (red-violet channel; 550-650 and red channel; 700-800 nm) as expected. The overlay of all channels is shown in the bottom panels for comparison. The scale bar is 50 μm.

## 4. CONCLUSIONS

In this project, we successfully developed a novel nanotool that is a Pdot-based nanoplatform for siRNA delivery. Positively charged Pdots with green (588 nm) and NIR (775 nm) fluorescence were synthesized and bound to negatively charged Control or Gapdh siRNA. Absorbance and surface properties of the Pdot-siRNA verified that siRNA was successfully conjugated with Pdots and the Pdots were readily taken up by brain-derived vascular cells. Further, the Pdot-siRNA had bright, stable fluorescence in two distinct emission wavelengths and the bound siRNA was able to inhibit target gene expression. A wide range of nanomaterials have been used to deliver small molecules, siRNA, and other proteins to cells[38, 39]; however, limitations in terms of toxicity, specificity or off-loading have remained a barrier to utilizing these tools more broadly. The novel Pdot-siRNA nanotool described herein represents a clear advantage for conducting dual imaging and gene expression inhibition in a variety of culture systems. The fact that the gene expression was successfully inhibited based on Gapdh protein immunolabeling intensity indicates that the Pdot-siRNA were taken up by the cells as a complex and that the siRNA was able to bind to its complementary target. It is not clear from the imaging whether or how long the Pdot remains associated with the siRNA once inside the cell; however, the siRNA are able to inhibit the target gene effectively. This offers the benefit of visualizing which cells have taken up the Pdot and the accompanying siRNA, further refining target-specific assessment and outcomes.

Although we used Gapdh as a proof-of-principle target in the current study, there are broader implications with regard to using this approach for other targets or for regulation of the Gapdh

gene expression, itself. Gapdh has been widely identified as playing a key role energy metabolism based on its ability to generate glyceraldehyde-3-phosphate and its contribution to a variety of cell processes[40]. Indeed, increased Gapdh gene expression and enzymatic function have been correlated with tumor cell proliferation owing to its enzymatic function for production of ATP and pyruvate under hypoxic microenvironmental conditions[41, 42]. By controlling Gapdh gene expression as a potential regulator of tumor cell death, this may serve as a new avenue for therapeutic targets. In a recent study with vascular EC, expression of the GAPDH gene was markedly increased under hypoxia stress[41]. The results of the current study lend support to the idea that not only can we deliver target-specific siRNA to cells, Gapdh in this case, but we can visualize exactly where and when the siRNA has been taken up. This type of multi-functional nanomaterial offers the advantage of imaging and targeted inhibition of gene expression in one small package.

ACKNOWLEDGMENTS

This work was supported by the NSF CHE NSF 2304873 (JXZ and DCD), NSF EPSCoR RII Track I Cooperative Agreement Award OIA-1946202; NIH COBRE grant (2P20GM104360-06A1; P.I. R. Vaughan); Multi-Investigator Seed Grant from the College of Arts and Sciences (J.X.Z. and D.C.D.), and a Pilot Project Grant from P20 GM104360 Epigenetics of Disease and Development (J.X.Z. and D.C.D.). Imaging studies were conducted at the UND Imaging Core facility, supported by NIH grant P20GM113123, DaCCoTA CTR NIH grant U54GM128729, and UNDSMHS funds. Research reported in this publication (RNA isolation and quality control) was conducted with the help of the UND Genomics Core, which is supported by the National Institute of General Medical Sciences of the National Institutes of Health under Award Number U54GM128729 and Award Number 2P20GM104360-06A1. The authors would like to express their sincere thanks to Elvira Tkach for technical assistance on this project.

REFERENCES

1. Ramjiawan, R. R.; Griffioen, A. W.; Duda, D. G., Anti-angiogenesis for cancer revisited: Is there a role for combinations with immunotherapy? *Angiogenesis* **2017,** *20* (2), 185-204.

2. Debela, D. T.; Muzazu, S. G.; Heraro, K. D.; Ndalama, M. T.; Mesele, B. W.; Haile, D. C.; Kitui, S. K.; Manyazewal, T., New approaches and procedures for cancer treatment: Current perspectives. *SAGE Open Med* **2021,** *9*, 20503121211034366.

3. Gupta, S. L.; Basu, S.; Soni, V.; Jaiswal, R. K., Immunotherapy: an alternative promising therapeutic approach against cancers. *Mol Biol Rep* **2022,** *49* (10), 9903-9913.

4. Li, T.; Kang, G.; Wang, T.; Huang, H., Tumor angiogenesis and anti-angiogenic gene therapy for cancer. *Oncol. Lett.* **2018,** *16* (1), 687-702.

5. Chen, X.; Mangala, L. S.; Rodriguez-Aguayo, C.; Kong, X.; Lopez-Berestein, G.; Sood, A. K., RNA interference-based therapy and its delivery systems. *Cancer Metastasis Rev* **2018,** *37* (1), 107-124.

6. Kim, B.; Park, J.-H.; Sailor, M. J., Rekindling RNAi Therapy: Materials Design Requirements for In Vivo siRNA Delivery. *Adv. Mater.* **2019,** *31* (49), 1903637.

7. Pittella, F.; Zhang, M.; Lee, Y.; Kim, H. J.; Tockary, T.; Osada, K.; Ishii, T.; Miyata, K.; Nishiyama, N.; Kataoka, K., Enhanced endosomal escape of siRNA-incorporating hybrid nanoparticles from calcium phosphate and PEG-block charge-conversional polymer for efficient gene knockdown with negligible cytotoxicity. *Biomaterials* **2011,** *32* (11), 3106-3114.

8. Xu, W.; Jiang, X.; Huang, L., 5.42 - RNA Interference Technology. In *Comprehensive Biotechnology (Third Edition)*, Moo-Young, M., Ed. Pergamon: Oxford, 2019; pp 560-575.

9. Wang, J.; Lu, Z.; Wientjes, M. G.; Au, J. L., Delivery of siRNA therapeutics: barriers and carriers. *Aaps j* **2010,** *12* (4), 492-503.

10. Sato, Y.; Matsui, H.; Sato, R.; Harashima, H., Neutralization of negative charges of siRNA results in improved safety and efficient gene silencing activity of lipid nanoparticles loaded with high levels of siRNA. *J Control Release* **2018,** *284*, 179-187.

11. Chen, Z.; Krishnamachary, B.; Pachecho-Torres, J.; Penet, M.-F.; Bhujwalla, Z. M., Theranostic small interfering RNA nanoparticles in cancer precision nanomedicine. *WIREs Nanomed. Nanobio.* **2020,** *12* (2), e1595.

12. Li, Y.; Ji, T.; Torre, M.; Shao, R.; Zheng, Y.; Wang, D.; Li, X.; Liu, A.; Zhang, W.; Deng, X.; Yan, R.; Kohane, D. S., Aromatized liposomes for sustained drug delivery. *Nat. Commun.* **2023,** *14* (1), 6659.

13. Seynhaeve, A. L. B.; Dicheva, B. M.; Hoving, S.; Koning, G. A.; ten Hagen, T. L. M., Intact Doxil is taken up intracellularly and released doxorubicin sequesters in the lysosome: Evaluated by in vitro/in vivo live cell imaging. *Journal of Controlled Release* **2013,** *172* (1), 330-340.

14. Yang, K.; Tran, K.; Salvati, A., Tuning Liposome Stability in Biological Environments and Intracellular Drug Release Kinetics. *Biomolecules* **2023,** *13* (1), 59.

15. Bharti, C.; Nagaich, U.; Pal, A. K.; Gulati, N., Mesoporous silica nanoparticles in target drug delivery system: A review. *Int J Pharm Investig* **2015,** *5* (3), 124-33.

16. Ajith, S.; Almomani, F.; Elhissi, A.; Husseini, G. A., Nanoparticle-based materials in anticancer drug delivery: Current and future prospects. *Heliyon* **2023,** *9* (11), e21227.

17. Thomas, T. J.; Tajmir Riahi, H. A.; Pillai, C. K. S., Biodegradable Polymers for Gene Delivery. *Molecules* **2019,** *24* (20), 3744.

18. Xia, W.; Tao, Z.; Zhu, B.; Zhang, W.; Liu, C.; Chen, S.; Song, M., Targeted Delivery of Drugs and Genes Using Polymer Nanocarriers for Cancer Therapy. *Int. J. Mol. Sci.* **2021,** *22* (17), 9118.

19. Zhou, R.; Zheng, Y.; Qian, L.; Yang, Y.; Holloway, P. H.; Xue, J., Solution-processed, nanostructured hybrid solar cells with broad spectral sensitivity and stability. *Nanoscale* **2012,** *4* (11), 3507-3514.

20. Darland, D. C.; Cain, J. T.; Berosik, M. A.; Saint-Geniez, M.; Odens, P. W.; Schaubhut, G. J.; Frisch, S.; Stemmer-Rachamimov, A.; Darland, T.; D'Amore, P. A., Vascular endothelial growth factor (VEGF) isoform regulation of early forebrain development. *Dev. Biol.* **2011,** *358* (1), 9-22.

21. Cain, J. T.; Berosik, M. A.; Snyder, S. D.; Crawford, N. F.; Nour, S. I.; Schaubhut, G. J.; Darland, D. C., Shifts in the vascular endothelial growth factor isoforms result in transcriptome changes correlated with early neural stem cell proliferation and differentiation in mouse forebrain. *Developmental Neurobiology* **2014,** *74* (1), 63-81.

22. Wu, C.; Bull, B.; Szymanski, C.; Christensen, K.; McNeill, J., Multicolor Conjugated Polymer Dots for Biological Fluorescence Imaging. *ACS Nano* **2008,** *2* (11), 2415-2423.

23. Rasband, W. In *ImageJ, U.S. National Institutes of Health, Bethesda, Maryland, USA*, 2011.

24. Perche, F.; Patel, N. R.; Torchilin, V. P., Accumulation and toxicity of antibody-targeted doxorubicin-loaded PEG–PE micelles in ovarian cancer cell spheroid model. *Journal of Controlled Release* **2012,** *164* (1), 95-102.

25. Kohay, H.; Sarisozen, C.; Sawant, R.; Jhaveri, A.; Torchilin, V. P.; Mishael, Y. G., PEG-PE/clay composite carriers for doxorubicin: Effect of composite structure on release, cell interaction and cytotoxicity. *Acta Biomaterialia* **2017,** *55*, 443-454.

26. Tian, G.; Pan, R.; Zhang, B.; Qu, M.; Lian, B.; Jiang, H.; Gao, Z.; Wu, J., Liver-Targeted Combination Therapy Basing on Glycyrrhizic Acid-Modified DSPE-PEG-PEI Nanoparticles for Co-delivery of Doxorubicin and Bcl-2 siRNA. *Frontiers in Pharmacology* **2019,** *10*.

27. Marasini, R.; Nguyen, T. D. T.; Rayamajhi, S.; Aryal, S., Synthesis and characterization of a tumor-seeking LyP-1 peptide integrated lipid–polymer composite nanoparticle. *Mater. Adv.* **2020,** *1* (3), 469-480.

28. Fotsing, P. N.; Woumfo, E. D.; Mezghich, S.; Mignot, M.; Mofaddel, N.; Le Derf, F.; Vieillard, J., Surface modification of biomaterials based on cocoa shell with improved nitrate and Cr(vi) removal. *RSC Adv.* **2020,** *10* (34), 20009-20019.

29. Park, J.; Shin, Y.; Won, W.; Lim, C.; Kim, J.; Kang, K.; Husni, P.; Lee, E.; Youn, Y.; Oh, K., Development of AE147 Peptide-Conjugated Nanocarriers for Targeting uPAR-Overexpressing Cancer Cells. *Int. J. Nanomedicine* **2021,** *16*, 5437-5449.

30. Zhao, B.; Kolibaba, T. J.; Lazar, S.; Grunlan, J. C., Environmentally-benign, water-based covalent polymer network for flame retardant cotton. *Cellulose* **2021,** *28* (9), 5855-5866.

31. Wu, C.; Chiu, D. T., Highly Fluorescent Semiconducting Polymer Dots for Biology and Medicine. *Angew. Chem. Int. Ed.* **2013,** *52* (11), 3086-3109.

32. Wu, X.; Chiu, D. T., Conjugated Polymer Nanoparticles and Semiconducting Polymer Dots for Molecular Sensing and In Vivo and Cellular Imaging. In *Conjugated Polymers for Biological and Biomedical Applications*, 2018; pp 59-85.

33. Gupta, N.; Chan, Y.-H.; Saha, S.; Liu, M.-H., Recent Development in Near-Infrared Photothermal Therapy Based on Semiconducting Polymer Dots. *ACS Applied Polymer Materials* **2020,** *2* (10), 4195-4221.

34. Patel, S.; Kim, J.; Herrera, M.; Mukherjee, A.; Kabanov, A. V.; Sahay, G., Brief update on endocytosis of nanomedicines. *Adv Drug Deliv Rev* **2019,** *144*, 90-111.

35. Ozel, I. O.; Ozel, T.; Demir, H. V.; Tuncel, D., Non-radiative resonance energy transfer in bi-polymer nanoparticles of fluorescent conjugated polymers. *Opt. Express* **2010,** *18* (2), 670-684.

36. Rajan, A. M.; Ma, R. C.; Kocha, K. M.; Zhang, D. J.; Huang, P., Dual function of perivascular fibroblasts in vascular stabilization in zebrafish. *PLoS Genet* **2020,** *16* (10), e1008800.

37. Caneparo, C.; Baratange, C.; Chabaud, S.; Bolduc, S., Conditioned medium produced by fibroblasts cultured in low oxygen pressure allows the formation of highly structured capillary-like networks in fibrin gels. *Scientific Reports* **2020,** *10* (1), 9291.

38. Mitchell, M. J.; Billingsley, M. M.; Haley, R. M.; Wechsler, M. E.; Peppas, N. A.; Langer, R., Engineering precision nanoparticles for drug delivery. *Nature Reviews Drug Discovery* **2021,** *20* (2), 101-124.

39. Luther, D. C.; Huang, R.; Jeon, T.; Zhang, X.; Lee, Y.-W.; Nagaraj, H.; Rotello, V. M., Delivery of drugs, proteins, and nucleic acids using inorganic nanoparticles. *Advanced Drug Delivery Reviews* **2020,** *156*, 188-213.

40. Bruns, G. A. P.; Gerald, P. S., Human Glyceraldehyde-3-Phosphate Dehydrogenase in Man-Rodent Somatic Cell Hybrids. *Science* **1976,** *192* (4234), 54-56.

41. Graven, K. K.; Troxler, R. F.; Kornfeld, H.; Panchenko, M. V.; Farber, H. W., Regulation of endothelial cell glyceraldehyde-3-phosphate dehydrogenase expression by hypoxia. *Journal of Biological Chemistry* **1994,** *269* (39), 24446-24453.

42. Nicholls, C.; Li, H.; Liu, J.-P., GAPDH: A common enzyme with uncommon functions. *Clinical and Experimental Pharmacology and Physiology* **2012,** *39* (8), 674-679.

# Data Availability Statements

The data supporting the findings of this study are available within the article and its supporting materials.